Interactions of positively and negatively charged iron-based engineered nanoparticles with organic matter: The case of humic acid

Malak Dia, Denis Courtier-Murias, Pierre-Emmanuel Peyneau, Béatrice Bechet

Interactions of Positively and Negatively Charged Iron-Based Engineered Nanoparticles with Organic Matter: The Case of Humic Acid †

Malak Dia,[‡,¶] Denis Courtier-Murias,[*,‡,¶] Pierre-Emmanuel Peyneau,[¶] and Béatrice Bechet[‡,¶]

‡*CNRS, ENSA Nantes, ECN, UGE, Nantes Université, La Rochelle Université, Le Mans Université, IMT Atlantique, Institut Agro Rennes Angers, CNAM, BRGM, AirPdL, CSTB, Cerema, ONIRIS, INRAE, Université Angers, Université de Caen Normandie, IRSTV, F-44300 Nantes, France.*

¶*Univ Gustave Eiffel, GERS-LEE, F-44344 Bouguenais, France.*

E-mail: denis.courtier-murias@univ-eiffel.fr

Abstract

The widespread release of engineered nanoparticles (NPs) into natural environments raises questions about the interactions of these colloids with natural organic matter (NOM), which directly influence their mobility, reactivity, and fate. While NP surface charge is recognized as a key factor in these interactions, evidence linking charge to molecular mechanisms remains limited. Cationic and anionic NPs were used in this study to investigate how NPs surface charge affects interactions with humic acid

†Electronic Supplementary Information (ESI) available

(HA), using fluorescence spectroscopy and dynamic light scattering (DLS). The results reveal that cationic NPs exhibit more important interactions with HA than anionic NPs, confirming that surface charge of NPs plays a key role on their interactions with HA. Complementary comparison showed that NP size and surface functionalization do not significantly impact these interactions, reinforcing surface charge as the important factor. Thermodynamic analyses at 270 nm, provide insights that these interactions involve carboxylic acid groups in HA. In addition, these analyses indicate that anionic NPs interact primarily through hydrogen bonding and Van der Waals forces. Finally, HA-NP interactions are more pronounced with an acidic pH than at neutral one, highlighting additional processes associated with charge modification.

Keywords

Nanoparticles, interactions, humic acid, coating, surface charge, environment.

Synopsis

Nanoparticle surface charge governs interactions with humic acid, affecting their environmental fate in natural waters and soils.

Highlights

- In this study, Cationic iron-based engineered nanoparticles interact more with humic acid than anionic ones.
- Nanoparticle size and coating had little effect on these interactions within the tested range.
- Anionic nanoparticles interact through hydrogen bonding and Van der Waals forces.
- Humic acid functional groups associated with the humic acid - nanoparticle interactions discernible at wavelength 270 nm are attributed to carboxylic acids.
- Higher interactions occur at pH 5 than at pH 7.

1. Introduction

In recent decades, nanotechnology has made huge advances, adding advancement across medicine [1], electronics [2], materials science, and urban applications [3, 4] . In light of these developments, engineered nanoparticles (NPs), which are known for their unique properties, are now produced and used widely [5]. However, this rapid increase in NP production has unavoidably led to their release into the environment, including air, water, and soil, during various stages of their life-cycle such as manufacturing, transport, use, and disposal. Pollutants, including NPs, are transported across different environmental compartments [6–8]. For instance, titanium (Ti)-bearing NPs emitted by anthropogenic sources have been found in various water bodies [9–13].

Once exposed to natural waters, NPs can interact with a wide range of environmental constituents, such as electrolytes, natural organic matter (NOM), inorganic matter, and anthropogenic pollutants [14–17]. Through a variety of physicochemical interactions, these constituents can affect the environmental fate and behavior of NPs. It has been shown that natural colloids, like NOM, which are frequently found in both terrestrial and aquatic environments, interact with NP [18–21]. It can for instance adsorb onto NP surfaces, altering its surface energy and reducing aggregation tendencies, as shown by Zhang et al. [21].

In recent years, numerous studies has been conducted in this area as a result of the increased interest in examining the interactions between different kinds of NPs and NOM [22–26]. However, despite this growing attention, our mechanistic knowledge of NOM–NP interactions is still fragmented and incomplete. The main limitation stem from the high heterogeneity present in both NOM and NPs. The composition of NOM, a complex mixture of organic compounds [27],varies greatly based on its source and the surrounding environment. Similarly, NP also vary in size, shape, surface charge, and chemical composition. To describe how NOM binds to or alters the surface properties of NPs, a number of mechanisms and adsorption models have been proposed [28]. These interactions are controlled by factors such as the chemical composition of NOM and NPs, their interfacial properties, and

environmental conditions like pH and ionic strength [28–32].

In this context, the surface coating of NPs, particularly through its surface charge and functionality, plays an important role in mediating interactions with colloidal substances such as NOM [31]. Indeed, these coatings act as the primary interface between NPs and environmental constituents, ultimately shaping their behavior and fate across natural and engineered systems [33–37].

Several studies have explored how NP coating materials affect their interactions with humic acid (HA), a major component of NOM. These studies often focus on the impact of coatings on NP stability and aggregation [38–44]. Recent findings from Sun et al. (2023) [45] showed that Fe_3O_4 NPs coated with different surface materials yet same charge interact distinctly with plant root exudates, affecting iron availability and uptake, highlighting the role played by surface coating in regulating NPs behavior in the plant rhizosphere. Despite these investigations, studies specifically addressing how charge variation introduced by coatings modulates molecular-level interactions with HA remain scarce [46]. Stankus et al. [46] examined the impact of five different coatings on gold (Au) NPs (anionic, cationic, and neutral coatings) on their interactions with model organic matter (Suwannee River Humic Acid) using zeta potential measurements. Their results showed that organic matter adsorbs onto Au NPs regardless of the coating used. However, the study did not observe significant variations in these interactions due to differences in surface charge, likely due to the limitations of relying solely on zeta potential measurements, which primarily provide information on surface charge and do not fully capture the complexity of the molecular interactions governing HA-NPs behavior. This complexity is also highlighted by the reactivity of HA, which is primarily driven by its diverse functional groups [47]. These reactive sites are crucial in determining HA interactions with NPs and other substances, influencing fundamental processes such as adsorption, stabilization, and complexation [48].

To address this challenge, this study employs fluorescence spectroscopy, which detects changes associated with specific functional groups and their local environment, thus captur-

ing a part of HA and its interactions and DLS which assesses size and aggregation behavior. Together, these techniques comprehensively investigate the effects of different NP surface charges on the interactions between NPs and HA under controlled physical conditions (i.e. pH and temperature). The investigation focuses on two pH levels, 7 and 5, at a temperature of 298 K. These values were selected to reflect environmentally relevant conditions of natural water systems such as surface water, and groundwater-bog water systems, respectively [49, 50]. Additionally, temperature variations at pH 7 have also been performed to further elucidate the physicochemical mechanisms driving these interactions. The study centers on two types of commercial iron-based NPs, each coated with dextran—a biocompatible polysaccharide recognized for its ability to stabilize NPs and modify their surface properties—and functionalized with distinct surface charges, one positive and the other negative. In addition, thermodynamic investigations will provide insights into the mechanisms driving HA-NP interactions, and the HA functional groups involved, contributing to enhance our understanding of the role of NPs surface charge in their environmental behavior. This work represents a controlled, model study that does not capture the full complexity of natural environmental systems, yet it helps understanding the mechanisms of interactions between positively and negatively charged NPs and HA.

2. Materials & Methods

2.1. Sample Preparation

Pahokee Peat HA, obtained from the International Humic Substances Society (IHSS, product number 1S103H), was used in this study. A 20 mg/L HA solution was prepared by dissolving 5 mg of HA in 250 mL of ultra-pure water. The pH of the solution was initially elevated to 12 using 1 M NaOH to ensure complete dissolution of HA. After achieving full dissolution, the pH was carefully readjusted to 7 or 5 using 1 M HCl to create the desired experimental conditions. Importantly, the NaOH and HCl were added without altering the

total volume of the solution, 100 µL and 80 µL, respectively, for an initial volume of 250 ml, ensuring that dilution effects were negligible.

Non-fluorescent iron-based NPs (BioPAL) were used. These NPs consist of an iron oxide (Fe_3O_4) core coated with a dextran layer yet functionalized differently to induce distinct charges. One type of NPs, functionalized with $C_2H_4NH_3^+$ (CL50Q02-2A), exhibits a positive charge (denoted as NPC^+), while the other has a negative charge, functionalized with hydroxyl groups (CL-30Q02-6) (denoted as NPC^-). Detailed characteristics (size and zeta potential) are provided in supplementary information (SI, Tab. S1).

To ensure reliable experimental conditions, the stability of the NPs at the selected pH levels was verified by measuring their zeta potential, confirming that they maintained consistent stability and charge throughout the experiments (see Fig. S1 & S2 for NPC^- and Fig. S3 & S4 for NPC^+). Additionally, zeta potential and size characterization of HA as a function of pH were conducted to gain insights into how HA behaves under different pH conditions. The results of these characterizations are discussed in detail in the subsequent section.

2.1.1. Fluorescence Spectroscopy Analysis

To investigate the interactions between HA and NPs, suspensions of NPC^+ and NPC^- at various concentrations (20, 40, 60, 80, 100, and 150 µM of Fe) were prepared by diluting stock NPs solutions into a 20 mg/L HA solution at pH 7 and 5. After 30 minutes of incubation following mixing (without agitation), each solution was analyzed using a fluorescence spectrophotometer (Cary Eclipse, Agilent) at two excitation wavelengths (λ = 270 nm and 460 nm), which are established reference values for HA excitation according to IHSS (Fig. S5). Both excitation wavelengths, 270 nm and 460 nm, have been associated with the excitation of carboxyl groups [22, 51] but it is well known that aromatic structures present in DOM (such as phenolic groups [52] and amino acids [53]) are also fluorescent. Thus, the precise identification and spatial distribution of the fluorescent groups within the HA structure, as

well as the specific chemical environments influencing their fluorescence, remain unclear [54]. Due to this ambiguity, we have chosen to proceed by studying the two fluorescent regions (270 nm and 460 nm), which represent two distinct parts of HA, without further assignment to specific functional groups or molecules. This still allows us to focus on the outcomes related to NP surface charge and to gain insights on the type of interactions.

Samples at pH 7 were also studied at different temperatures (298, 318, and 338 K) to gain deeper insight into the interactions between NPs and HA, whether they are static or dynamic, and to identify the type of bonding involved. Since it was not possible to control the temperature during fluorescence analysis, 10 mL the samples were preheated in a water bath before measurement. From each sample, 3 mL taken from the middle were transferred into the instrument for analysis. As each fluorescence analysis lasted approximately two minutes, only minor temperature fluctuations were expected during sample preparation.

2.1.2. Dynamic Light Scattering Analysis

DLS analysis was performed using a Zetasizer Ultra (Malvern) to observe any potential modifications in HA sizes upon the addition of NPs at pH 7. To achieve this, NPC^+ was selected as the focus of the analysis.

The first step was to determine the concentration of NPC^+ that would not interfere with HA measurements. This was accomplished by evaluating the size of NPC^+ at various concentrations (20 - 9000 µM) in a 1 mM KCl solution at pH 7. At 20 µM, the correlogram revealed weak diffusion (diffusion coefficient < 0.6), indicating that the NP were too dilute to be reliably detected. This result confirmed that concentrations at or below 20 µM would not significantly interfere with HA detection.

Following this, HA samples at 20 mg/L were prepared with NPC^+ at concentrations of 5, 10, and 15 µM of Fe under controlled conditions of pH 7 and 298 K.

2.2. Fluorescence spectroscopy data analysis

If NPs interact with HA, a decrease in the initial fluorescence intensity of HA, known as quenching, is expected. The relationship between the fluorescence intensity of the fluorophore, HA in our case, and the concentration of the quenching agent, the substance that reduces fluorescence intensity, NPs in our case, is described by the Stern-Volmer equation (Eq. 1), which is used to study the interaction dynamics between the fluorescent emitter and the quencher [55]. This equation describes the evolution of the fluorescence intensity ratio as a function of the quencher concentration [Q],

$$\frac{\mathrm{I}_0}{\mathrm{I}} = 1 + K_{SV}\,[Q], \tag{1}$$

where I_0 and I denote, respectively, the HA intensities before and after the addition of NPs. K_{SV} represents the Stern-Volmer constant.

Fluorescence quenching, as outlined by the Stern-Volmer theory (Eq. 1), typically presents a linear plot, indicating either a dynamic or static quenching process [55–57]. Static quenching occurs when a non-fluorescent complex forms between the fluorophore and quencher molecules in their ground state before the excitation. On the other hand, dynamic quenching, also known as collisional quenching, occurs when the quencher interacts with the fluorophore while it is in its excited state, which typically happens shortly after the fluorophore absorbs light and transitions from its ground state to a higher energy state. Since both types of quenching produce linear plots, distinguishing between them solely through fluorescence intensity measurements cannot be done. Temperature studies help differentiate between quenching mechanisms. Typically, dynamic quenching is characterized by a steeper slope on the Stern-Volmer plot, which is caused by an increase in temperature that intensifies collisional quenching between the quencher and the excited fluorophore. On the other hand, static quenching implies the quencher and the fluorophores forming a stable ground-state complex. In general, temperature has little effect on static quenching because the complex

stays stable. However, if the complex destabilizes, the quenching efficiency decreases, which results in a smaller slope on the Stern-Volmer plot [55].

While the Stern-Volmer equation typically predicts a linear relationship between fluorescence intensity and quencher concentration, this is not always the case. Deviations from linearity behavior can occur [55, 58]. An upward curvature indicates the simultaneous presence of both static and dynamic quenching processes contributing to the decrease in fluorescence intensity [55, 59]. A downward curvature or negative deviation from the linearity can also be observed in Stern-Volmer plots [55, 59, 60]. These deviations from linearity underscore the complexity of quenching mechanisms, where the presence of multiple fluorophores or combined quenching processes necessitates a more detailed analysis to accurately interpret fluorescence data.

2.3. Binding Mechanisms

For interactions involving a static quenching mechanism, the quencher (Q) forms a stable, non-fluorescent complex with the fluorophore (F), as described by the equilibrium equation:

$$F + nQ \rightleftharpoons FQ_n$$

To analyze the binding interactions, the double logarithmic equation can be applied [61–63]:

$$\log\left(\frac{I_0 - I}{I}\right) = \log K + n\log[Q] \tag{2}$$

In this context, $[Q]$ represents the concentration of the quencher available for binding to the target site on the fluorophore. However, not all quencher molecules may be free; some could be bound to other sites that do not contribute to the observed quenching at the measured wavelength. Given this, the initial quencher concentration $[Q]_0$ is used as an approximation for the concentration of the quencher specifically involved in the binding

interaction under study. This assumption simplifies the analysis, allowing the focus to remain on the primary binding interaction of interest. The validity of this approximation is supported by a linear relationship obtained by plotting $\log\left(\frac{I_0-I}{I}\right)$ against $\log[Q]_0$. In this plot, the slope indicates the stoichiometry of the binding interaction (n) for the functional groups measured at the specified wavelength, while the intercept provides the logarithm of the binding constant (K) for these same functional groups involved in the interaction [64].

Building on this characterization, the possible nature of interaction between the NPs and the HA — such as electrostatic forces, hydrophobic interactions, hydrogen bonding, and Van der Waals forces — can be further deduced by examining the thermodynamic parameters of the interactions [61–63, 65, 66]. Assuming that ΔH and ΔS remain constant when the temperature does not vary significantly [63], these parameters can be determined using the Van 't Hoff equation (Eq. 4) [62, 65, 67],

$$\ln K = -\frac{\Delta H}{RT} + \frac{\Delta S}{R} \tag{3}$$

with R representing the universal gas constant.

3. Results and discussion

3.1. Influence of coating on interactions

The fluorescence emission intensity of HA at pH 7 and 298 K (conditions that can met the environment) was recorded in the presence of increasing concentrations of both negatively and positively charged NPs (Fig. 1 for 270 nm and Fig. S6 for 460 nm).

For both types of NPs and at both excitation wavelengths, the impact of NPs on the emission intensity of HA increases as the concentration of NPs rises. This effect is characterized by a noticeable decrease in HA emission intensity, while the emission maximum λ and band shapes remain unchanged. Given that these NPs are non-fluorescent, the observed de-

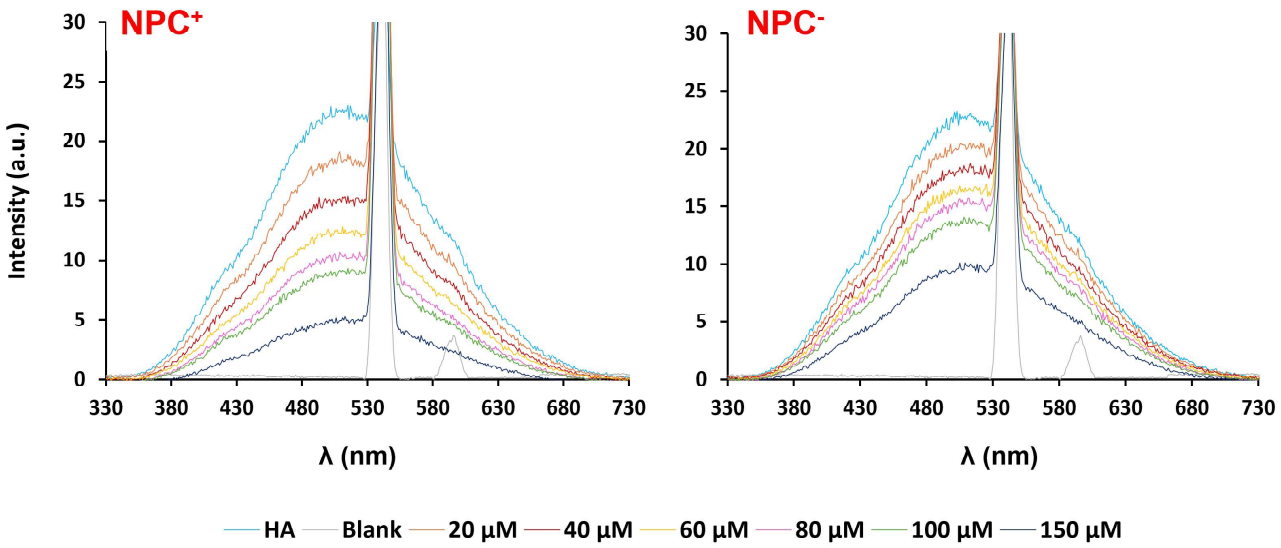

Figure 1: Emission spectra of HA excited at 270 nm as a function of NP concentration at pH 7 and T = 298 K.

crease in HA emission intensity can be attributed to direct interactions between HA and the NPs [22, 38, 68, 69]. Notably, for the same concentration of NPs (either NPC^+ or NPC^-), the quenching effect is more pronounced at 270 nm than at 460 nm. This suggests that the functional groups excited at 270 nm either have a stronger intrinsic affinity with NPs or are more accessible to the NPs than those excited at $\lambda = 460$ nm.

Comparing the quenching effects between the two types of NPs at equal concentrations, the fluorescence intensity of HA shows a more significant decrease in the presence of NPC^+, the positively charged NPs, compared to NPC^-, which are negatively charged. Additional comparisons, presented in the SI (section E), discard the importance of NPs size and surface functional groups, validating the fact that surface charge plays a key role on the interactions of NPs with HA. This was done by comparing NPC^- (60 µM) with two other negatively charged iron-based NPs—NPCO and NPAm 20 nm each— (Fig. S7-8) under identical experimental conditions. All three NPs induced a similar decrease in HA fluorescence intensity as shown in Fig 2, reinforcing the idea that surface charge, rather than NP size or surface functionalization, governs the interaction with HA - further discussion provided in the SI

(section E). These findings show experimentally, for the first time, the importance of the charge-dependent nature of the interactions between HA and the NPs.

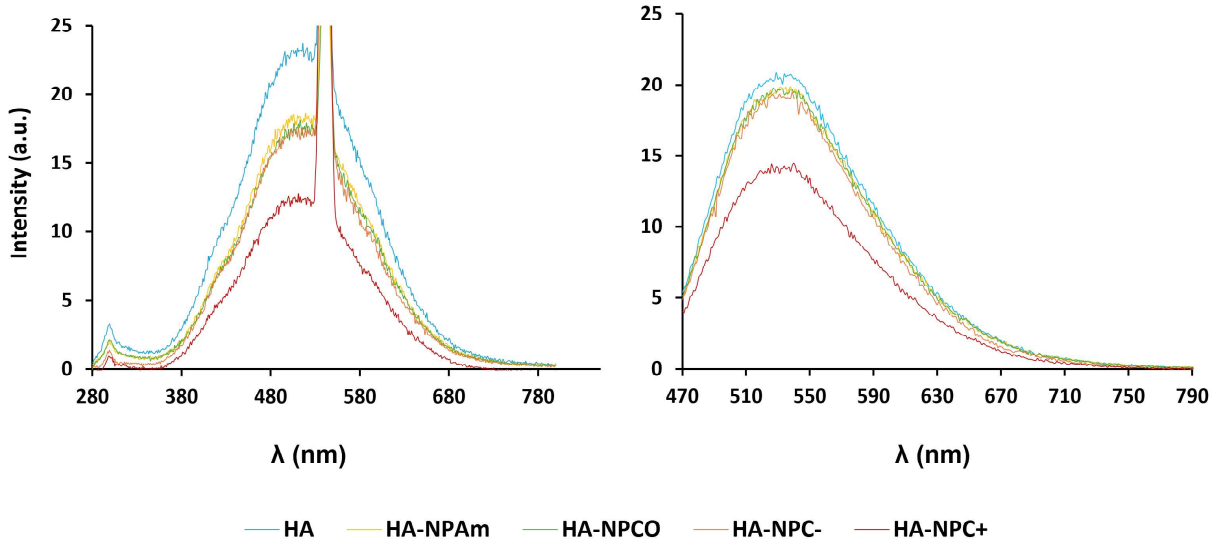

Figure 2: Emission spectra of HA excited at 270 nm and 460 nm as a function of NP type at 60 µM, pH 7, and T = 298 K.

3.2. Characterizing the interactions

Emission spectra (Fig. 1) for both NPs and excitation levels have been fitted to the Stern–Volmer equation (Eq. 1). The ratio I_0/I plotted as a function of NPs concentration at each excitation level is represented below (Fig. 3).

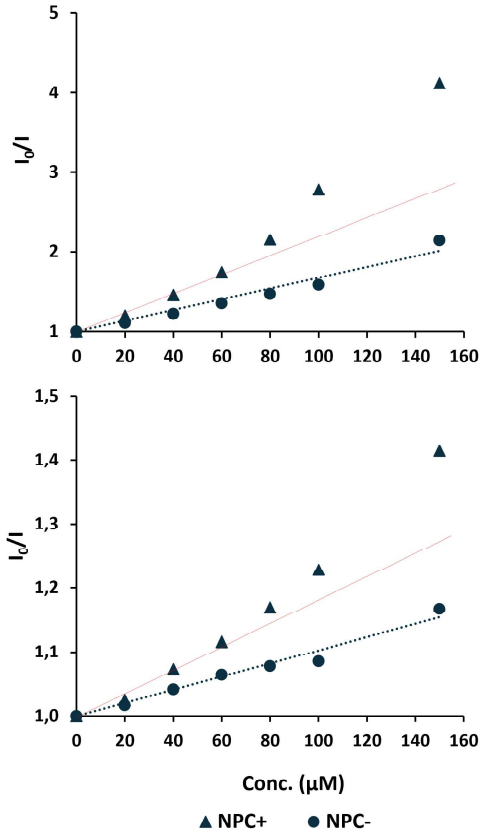

Figure 3: Stern-Volmer plot of NPC^+ and NPC^- at pH 7 and T = 298 K. The lines correspond to the linear fit across the entire concentration range (0 to 150 µM) for NPC^- and for the three lowest concentrations (20, 40, and 60 µM) for NPC^+.

Starting with NPC^+, the plot shows good linearity at low concentrations (0-60 µM) across both excitation levels. This linearity suggests that, within this range, an interaction occurred between NPC^+ and the functional groups associated with 270 and 460 nm. This interaction is either mediated by a static or a dynamic quenching process [55, 70, 71]. However, as concentrations exceed this range, an upward curvature begins to emerge when compared to the fit of the lower concentrations (red line). This deviation indicates a change in the interaction process, suggesting that at higher concentrations, the system transitions to a more complex interplay that incorporates both static and dynamic quenching processes.

NPC^-, on the other hand, shows a different behavior. The plots display a consistent linearity across the entire concentration range and at both excitation wavelengths, indicating

that the interactions systematically follow either a static or a dynamic quenching process at all studied concentrations.

3.2.1. HA-NP interaction: static or dynamic?

Further fluorescence experiments were conducted on pH 7 samples, yet this time at different temperatures, to investigate the nature of the interactions, whether static or dynamic. It should be noted that temperature fluctuations due to the experimental protocol reduce the accuracy of Stern-Volmer constants but still allow to observe qualitative trends to differentiate between static and dynamic interactions (see section H in SI for further details).

First, a slight decrease in HA emission intensity has been observed in the absence of NPs with increasing temperatures, particularly at 270 nm (Fig. S9); however, this change appears to be minimal. Accordingly, the systems can be effectively compared at 298, 318, and 338 K. Upon the addition of NPs, the emission spectra of HA at both excitation levels and for both types of NPs consistently exhibited a reduction in intensity with increasing NPs concentration, indicating that quenching persists despite the temperature rise. Notably, NPC^+ continued to induce a greater decrease in HA intensity compared to NPC^-, a trend consistent with observations at ambient temperature.

To further examine the nature of these interactions, the I_0/I ratio was plotted as a function of NPs concentration and compared with the data obtained at 298 K (Fig. S10 & S11). The corresponding Stern-Volmer constants for both NPs - calculated within the linearity ranges - at three temperatures and both excitation levels are summarized in the Tab. 1.

Upon increasing the temperature from 298 K to 338 K in the presence of NPC^-, a significant reduction in the I_0/I ratio is observed at both excitation levels. This decrease clearly shows that the interaction between NPC^- and the associated functional groups at 270 and 460 nm follows a static quenching, which entails the formation of a non-fluorescent ground-state complex. Additionally, this decrease of the Stern-Volmer constant indicates

Table 1: Stern-Volmer constants as function of temperature at pH 7.

NPs	T (K)	K_{SV} 270 (mM^{-1})	R^2	K_{SV} 460 (mM^{-1})	R^2
NPC^-	298	6.7	0.96	1	0.97
	318	5.4	0.89	0.5	0.71
	338	5.1	0.88	0.5	0.66
NPC^+	298	12.0	0.99	1.9	0.97
	318	12.6	0.99	2.5	0.99
	338	12.7	0.98	3.5	0.97

that quenching is less effective at higher temperatures than it is at ambient temperature. This suggests that the complex produced by NPC^- and the functional groups of interest on HA is most likely formed by weak binding forces which are sensitive to temperature increase. As the temperature rises, these bonds can break, making the complexes less stable, resulting in a decreased quenching effect.

In contrast, the interaction of NPC^+ with the same functional groups of interest on HA shows a distinct trend. At 460 nm, the I_0/I ratio increases with temperature from 298 K to 338 K, showing that the interaction between functional groups associated with this wavelength and NPC^+ is driven by dynamic (or collisional) quenching. In this case, the functional groups in their excited state at 460 nm interact with NPC^+, forming a complex. As the temperature increases, the enhanced molecular mobility of HA promotes more frequent collisions, resulting in a stronger quenching effect compared to that observed at ambient temperature. Building on this observation, it can be inferred that under real-world conditions, environmental factors—particularly sunlight exposure—could excite functional groups that absorb at 460 nm, as sunlight spans a broad spectrum, including visible wavelengths where 460 nm falls within the blue region. This excitation would facilitate dynamic interactions with positively charged NPs like NPC^+.

At 270 nm, however, clear differences are visible. The I_0/I ratio for NPC^+ remains nearly constant as the temperature increases, exhibiting minimal variation. This stability indicates that the interaction between the functional groups associated with the 270 nm and NPC^+ forms a stable complex, resistant to temperature changes. The persistence of the quenching

effect at this wavelength, despite the temperature increase, indicates that the interaction is governed by a static quenching mechanism rather than dynamic one. Such stability, in turn, suggests the presence of strong binding between these functional groups and NPC^+.

This behavior contrasts with observations at 460 nm, where collisional interactions take place. These results highlight that the interaction between HA and positively charged NPs (e.g. NPC^+) can involve distinct interaction mechanisms depending on the functional groups involved and their excitation state.

3.2.2. Mechanism driving the binding forces at environmental conditions

Ross and Subramanian [67] investigated the thermodynamic parameters involved in protein association processes. Their findings showed that hydrophobic forces are characterized by both positive ΔH and ΔS; Van der Waals interactions and hydrogen bond formation are characterized by both negative ΔH and ΔS. Electrostatic interactions are associated with extremely small ΔH (either sign) and a positive ΔS.

Therefore, despite the potential temperature instability during sample preparation, the thermodynamic parameters ΔH and ΔS for interactions involved in static processes, thus excluding NPC^+ at 460 nm, are calculated using Eq. 3. Given the complexity of the system, caution should be taken when interpreting ΔH and ΔS, as these values may be influenced by multiple competing factors, such as solvation effects [72]. Thus, these parameters, will offer qualitative insights into the binding mechanisms between HA – particularly with functional groups associated with 270 and 460 nm – and NPs at pH 7 (Tab. 2).

Table 2: Thermodynamic parameters of the static interactions between HA and NPs.

NPs	λ (nm)	T (K)	K (L/mol)	R^2	ΔH (kcal/mol)	ΔS (cal/(mol.K))	R^2
NPC^-	270	298	3.43 x 10^3	0.99	-15.37	-46.10	0.90
		318	1.73 x 10^2	0.99			
		338	9.11 x 10^1	0.99			
	460	298	7.31 x 10^2	0.98	-59.44	-226.01	0.98
		318	8.35 x 10^{-2}	0.98			
		338	5.35 x 10^{-4}	0.98			
NPC^+	270	298	2.60 x 10^3	0.99	1.92	23.36	0.96
		318	3.58 x 10^3	0.98			
		338	4.10 x 10^3	0.99			

Starting with NPC^-, the results show negative values for both ΔH and ΔS at both excitation levels. The negative ΔH indicates that the interaction is exothermic, meaning that the binding process releases heat. On the other hand, the negative ΔS suggests a decrease in disorder during the binding process, which could result from the ordering of solvent molecules or the alignment of the interacting molecules as the complex forms. These thermodynamic characteristics are consistent with interactions involving hydrogen bonds and/or Van der Waals forces [67]. This reinforces the earlier hypothesis that weak binding forces, such as hydrogen bonding and Van der Waals interactions, play a role in the interaction between NPC^- and the functional groups associated with 270 and 460 nm. In line with these findings, as the temperature increases, a noticeable decrease in the binding constant K is observed at both wavelengths, indicating a decrease in binding affinity. This reduction is attributed to the weakening of hydrogen bonds and Van der Waals interactions, which are particularly sensitive to thermal energy. In a similar context, Loosli et al. [73] studied the interaction between TiO_2 engineered NPs and HA using isothermal titration calorimetry. They revealed that the binding interactions were driven by Van der Waals forces, particularly due to the amphiphilic character of HA. Their observations support the findings of our study, where Van der Waals forces and hydrogen bonding are identified as contributors to the binding interactions between NPC^- and HA.

For NPC^+ at 270 nm, the results reveal a slight positive ΔH and positive ΔS. The

positive ΔH indicates that the interaction is endothermic, meaning that the binding process requires the absorption of heat. On the other hand, the positive ΔS suggests a net increase in disorder, which could result from the release of water molecules or counter-ions during complex formation. These observations point to the contribution of electrostatic binding forces [67]. Given that electrostatic forces are relatively strong interactions, this supports the hypothesis regarding the stability of the complex formed between the functional groups associated with 270 nm and NPC^+. Furthermore, the increase in the binding constant K with rising temperature provides additional support for the endothermic nature of the interaction. This suggests that the binding interaction becomes more favorable as heat is absorbed.

Since there are mostly electrostatic interactions between NPC^+ and the functional group at 270 nm, we can say that this functional group has a negative charge. Researchers are still trying to figure out the exact chemical structure of HA because it is so complicated and varied. However, it is well known that HA has a lot of carboxyl (R–COOH), nitrogen-containing ($R–NH_2$), and phenolic groups [74]. At pH 7, HA predominantly carries a negative overall charge, primarily due to the deprotonation of its carboxyl groups, which have a pKa around 4, leading to the formation of carboxylate groups (COO^-) [75, 76]. Phenolics, on the other hand, have a pKa around 9 [76], which means that at pH 7, they stay mostly protonated (neutral). Our zeta potential analysis of HA at pH 7 (Fig. S12) confirms the presence of two distinct zeta potential values (positive and negative), with the negative value being more prominent. It is thus hypothesized that the ionized carboxyl groups have an important contribution to the 270 nm absorption. In light of these results, the electrostatic interaction between NPC^+ and HA at 270 nm should be driven by the attraction between the RNH_3^+ groups on NPC^+ and the carboxylate groups on HA. On the other hand, at the same excitation wavelength, the hydroxyl groups on NPC^- exhibit a weaker affinity for the carboxylate groups, likely forming hydrogen bonds between the hydrogen atom of the hydroxyl group and the oxygen atom of the carboxyl groups. This interpretation is consistent with the

thermodynamic data obtained; however, given the limitations of fluorescence in providing detailed information about functional groups, further research using complementary techniques such as FTIR, NMR, or XPS is required to confirm these hypotheses. For instance, recent developments in NMR have demonstrated its potential for studying the interactions between NPs and humic acid, although it has yet to be applied under relevant environmental conditions [77]

3.3. Impact of pH on the interactions

To better understand the interaction between HA and NPs, complementary fluorescence analyses were performed on the HA and HA-NP samples at the same concentrations, this time at pH 5 and 298 K. The results were then compared with those obtained at pH 7. Initial observations revealed a decrease in the emission intensity of HA at pH 5 at both excitation levels (Fig. 4). This reduction in intensity could be attributed to an increased protonation of functional groups at lower pH and/or a change in the conformation of HA, which may affect the electronic structure of fluorescent HA and reduce fluorescence efficiency.

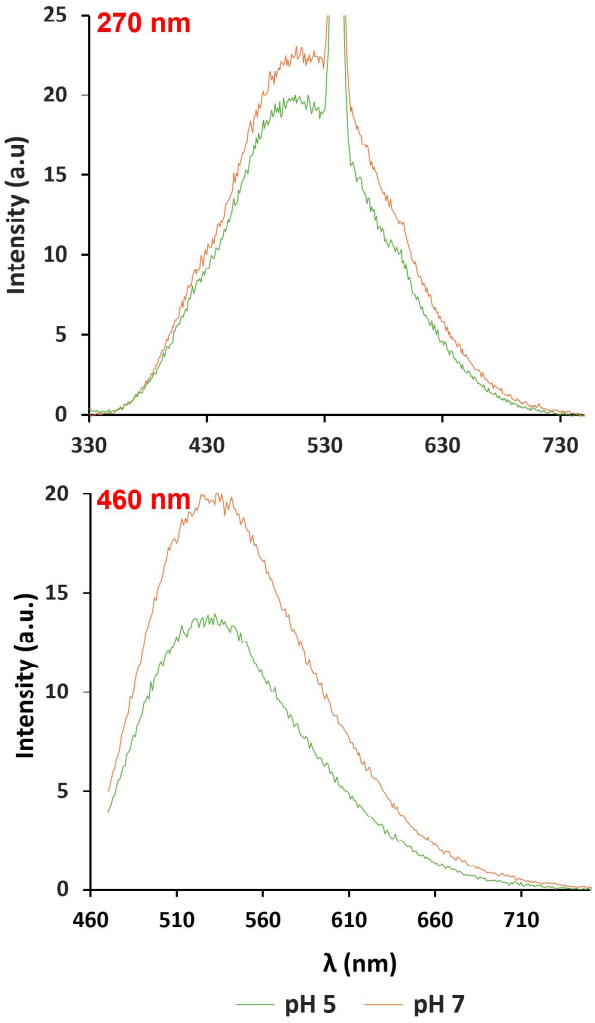

Figure 4: Emission spectrum of HA at $\lambda = 270$ and 460 nm for pH = 5 and pH = 7.

Following this observation, the zeta potential and hydrodynamic size of HA (at the same concentration of 20 mg/L) over a pH range between 2 and 10 were measured. The zeta potential results (Fig. S13) showed that HA remained with an overall negative charge whatever the pH, the zeta potential shifted from around -40 mV at pH $>$ 5 to around -25 mV at pH 4 and below. This behavior is consistent with a study by Stankus et al. [46], which demonstrated that HA retains an overall negative charge across a pH range from 2 to 10. In addition, the analysis of the zeta potential distributions (Fig. S14) revealed that the absolute values of both the positive and negative regions decreased as the pH decreased. Furthermore, the two regions became closer to each other. This could indicate a reduction in overall charge density, likely due to the increased protonation of functional groups at lower pH.

Such changes in protonation could also lead to conformational changes in HA [78], which may affect the accessibility and distribution of functional groups, further contributing to the reduction in charge disparity between the positive and negative regions. Indeed, the hydrodynamic size distribution of HA (Fig. S15) reveals a shift toward larger size diameters as the pH value decreases, suggesting the possibility of aggregation occurring within the HA. At the same time, smaller HA components become observable at lower pH, likely as a result of an aggregation effect. Further discussions about these results can be found in the SI. This increase in size is in agreement with a recent study by Tu Luan et al. [78] in which it was reported that HA structures tend to be thread-like at high pH, whereas at low pH it aggregates into droplet-like structures yielding an increase in diameter in DLS measurements. In line with these findings, a study [79] reported that micelle-like aggregation and the interfacial adsorption of HA were substantially facilitated in the acidic region. This aggregation behavior supports the hypothesis that conformational changes in HA, as indicated by the zeta potential distribution, may be occurring.

After introducing the NPs, the interaction between HA and the NPs is again (as for pH 7) more pronounced with NPC^+ at pH 5 compared to NPC^-, indicating that the interaction

order is not affected by the conformational changes in the HA structure. The I_0/I ratios as a function of NP concentration for both samples at pH 5 were used to obtain the Stern-Volmer constants and compared to the corresponding values at pH 7 (cf. constants reported in Tab. 3).

Table 3: Stern-Volmer constants for pH 5 and 7 at 298 K.

NPs	pH	K_{SV} 270 nm (mM^{-1})	K_{SV} 460 nm (mM^{-1})
NPC^-	7	6.7	1.0
	5	7.9	1.6
NPC^{+*}	7	12.0	1.8
	5	12.8	3.5

**: Slopes are calculated within the linearity domain (0-60 μM)*

At pH 5, more protonation of carboxyl groups absorbing at 270 nm is expected, which would reduce their capacity to interact with positively charged NPs. This effects led to the expectation that the overall interaction strength at pH 5 would be lower compared to that observed at pH 7. However, surprisingly, the experimental results revealed a contrasting trend. The observed Stern-Volmer constants (K_{SV}) at pH 5 are higher for both excitation wavelengths (270 nm and 460 nm) and for both types of NPs compared to those measured at pH 7. This enhancement in interaction strength is especially pronounced for functional groups absorbing at 460 nm. These results indicate that the acidic environment promotes stronger interactions between HA and the NPs, a finding that was unexpected, particularly for carboxyl groups absorbing at 270 nm. Under normal conditions, protonation at acidic pH would be expected to weaken interactions with positively charged NPs due to reduced electrostatic attraction.

The discrepancy between expected and observed behavior indicates that additional factors beyond simple protonation are influencing the interactions. A key factor is the aggregation and structural reorganization molecules at pH 5. Such reorganization can exposes previously inaccessible functional groups, increasing their availability for interaction with the NPs. This structural rearrangement particularly affects the functional groups associ-

ated with absorption at 460 nm, amplifying their interactions under acidic conditions. A study by Xie et al. 2020 [80] demonstrated using chemical force microscopy that HA binding to surfaces is governed by electrostatic forces, hydrophobic interactions, and hydrogen bonding, all of which vary with pH and ionic strength. Notably, the adhesion of HA to amino-functionalized surfaces was shown to reverse from attraction to repulsion under alkaline pH conditions, which align to what we observed in our study.

This behavior mirrors findings from other studies that highlight the complex nature of interactions between dissolved organic matter, such as HA, and contaminants. For instance, a study on HA and various xenobiotics revealed that pH significantly influences binding interactions due to conformational changes in the HA structure. Specifically, at high pH, HA structures open up, making functional components more accessible for interactions with contaminants [81]. Similarly, another study investigating bisphenol A binding to HA across a broad pH range found that pH modulates both the strength and type of interactions [62]. While these studies observed pH-dependent behavior in the binding of organic contaminants to HA, our results present a distinct trend—enhanced interactions at pH 5, which suggests that NPs may behave differently compared to organic contaminants in acidic conditions.

These findings highlight the complex nature of HA-NPs interactions, which cannot be explained solely by pH-induced protonation effects. The observed increase in interaction strength at pH 5 emphasize the role of structural and molecular rearrangements of HA under acidic conditions. This suggests that future studies should consider not only chemical modifications but also conformational dynamics of HA in different environmental contexts, as both factors may significantly influence the behavior of HA in relation to nanoparticles and other pollutants.

3.4. Influence of NPC^+ on HA size

Fluorescence analysis revealed that NPC^+ interacts more strongly with the functional groups of interest in HA compared to NPC^-. Building on this finding, the next step was to

investigate how NPC^+ affects the size distribution of HA molecules at pH 7 and 298 K.

To begin, the size distribution of HA in the absence of NPs was first analyzed. The results (Fig. S16) revealed three distinct peaks: Peak A around 10 nm, Peak B near 100 nm, and Peak C at approximately 700 nm, reflecting the presence of HA molecules in various aggregate sizes.

Next, we determined the minimal concentration of NPC^+ required to avoid interference with HA size measurements by testing a range of concentrations from 900 µM to 20 µM. As the concentration of NPC^+ decreased, the correlation coefficient of the correlogram (Fig. S17) also dropped. At 20 µM, the correlogram revealed weak diffusion (coefficient < 0.6), indicating that the NPs were too dilute to be detected accurately. Thus, this concentration is low enough to ensure accurate detection of HA behavior without significant interference. As such, concentrations below 20 µM of NPC^+ will not substantially affect HA size measurements.

With this threshold established, we next introduced NPC^+ at intermediate concentrations of 5, 10, and 15 µM. At these concentrations, noticeable changes in the HA size distribution were observed. The intensity of Peak A increased, indicating a rise in the number of smaller HA aggregates. In contrast, Peak B showed a significant decrease in intensity as the concentration of NPC^+ increased. This indicates that mid-sized HA aggregates are being disrupted and broken down into smaller particles, resulting in a higher concentration of smaller-sized particles, as reflected by the increased intensity of Peak A. Meanwhile, Peak C, which represents the largest HA aggregates, exhibited a slight decrease in intensity upon the addition of NPC^+ (especially at 15 µM). Although this reduction was less pronounced than the changes in Peaks A and B, it suggests that even the largest HA aggregates are somewhat affected by NPC^+.

This disruption is probably caused by the interaction between the negatively charged carboxylate (COO^-) groups on HA and the RNH_3^+ groups on the surface of NPC^+, which could potentially break down HA aggregates and cause structural modifications. This finding

is in line with a previous study [82] that found that citrate-coated gold NPs caused HA to break up significantly. This was probably because they changed the hydrogen bonds in HA aggregates and made it easier for HA molecules and gold NPs to exchange ligands. Brigante et al. [83] and Piccolo et al. [84] also found that monocarboxylic acids caused HA aggregates to break apart. They proposed that humic substances (HS) are groups of smaller molecules that are held together by hydrophobic forces. When carboxylic acids come into contact with HS, these forces can be broken, which causes the HS to break apart into smaller molecules. In the current study, the interaction between NPC^+ and HA probably works in a similar way, though driven by electrostatic interactions. In this case, the RNH_3^+ groups probably break up existing bonds and forces in HA, which leads to changes in the HA structure.

4. Conclusion

This study focuses on the interaction between positively and negatively charged NPs with humic acid. It offers new insights into these interactions showing that they are influenced by the charge of the NPs involved but also some functional groups of HA (which has been assigned to carboxyl groups). Fluorescence analysis, showed that both positively and negatively charged NPs can form complexes with HA, and that the interactions between positively charged NPs and HA functional groups are more important than those observed with negatively charged NPs. This suggests that NPs with a positive charge might have higher affinity for natural organic matter in the environment.

According to fluorescence experiments, positively charged NPs interact with HA via different mechanisms: static quenching happens when groups absorb at 270 nm, whereas dynamic quenching is linked to groups that absorb at 460 nm and frequently requires external stimuli like light. This suggests that, depending on the environment and the availability of functional groups, HA and positively charged NPs can coexist with several quenching mechanisms, both static and dynamic, either independently or simultaneously. Furthermore, the

conclusion of this study are in agreement to previous works suggesting that the functional groups associated with the 270 nm absorption are carboxyl groups, contributing to a better understanding of the specific interactions between NPs and HA. Additionally, environmental factors such as pH, temperature, and light intensity can also influence the interactions between HA and NPs. While these results are important, using additional techniques such as FTIR and NMR are recommended to improve understanding of the underlying mechanism.

Finally, the formation of HA-NPs complexes highlighted in this study raises concerns about the potential of NPs associated with environmental risks. When NPs interact with HA or NOM, these complexes can alter their properties, such as size, solubility, and aggregation, making them more likely to be unintentionally removed or overlooked during sampling and standard preparation methods such filtration. This may result in an underestimation of the concentrations of NPs in the environment. Therefore, it is important to continue to consider the intricate interactions, at the molecular-level, between NPs and NOM like HA in environmental assessments.

Acknowledgement

This work has benefited from the 2020 CNRS – University of Toronto Joint Call for PhD Mobility Funding Programme supporting Malak Dia.

References

(1) Rahman, M.; Akhter, S.; Ahmad, M. Z.; Ahmad, J.; Addo, R. T.; Ahmad, F. J.; Pichon, C. Emerging advances in cancer nanotheranostics with graphene nanocomposites: opportunities and challenges. Nanomedicine **2015**, 10, 2405–2422.

(2) Payal; Pandey, P. Role of Nanotechnology in Electronics: A Review of Recent Developments and Patents. Recent Patents on Nanotechnology 16, 45–66.

(3) de la Fuente, J. M.; Penadés, S. Glyconanoparticles: Types, synthesis and applications in glycoscience, biomedicine and material science. Biochimica et Biophysica Acta (BBA) - General Subjects **2006**, 1760, 636–651.

(4) Hernández-Moreno, S. Handbook of Nanomaterials and Nanocomposites for Energy and Environmental Applications; Springer, 2021; pp 2747–2765.

(5) Parveen, K.; Banse, V.; Ledwani, L. Green synthesis of nanoparticles: Their advantages and disadvantages. AIP Conference Proceedings **2016**, 1724, 020048.

(6) Zgheib, S.; Moilleron, R.; Chebbo, G. Priority pollutants in urban stormwater: Part 1 – Case of separate storm sewers. Water Research **2012**, 46, 6683–6692.

(7) Opher, T.; Friedler, E. Factors affecting highway runoff quality. Urban Water Journal **2010**, 7, 155–172, Publisher: Taylor & Francis _eprint: https://doi.org/10.1080/15730621003782339.

(8) Markiewicz, A.; Björklund, K.; Eriksson, E.; Kalmykova, Y.; Strömvall, A.-M.; Siopi, A. Emissions of organic pollutants from traffic and roads: Priority pollutants selection and substance flow analysis. Science of The Total Environment **2017**, 580, 1162–1174.

(9) Wang, J.; Nabi, M. M.; Erfani, M.; Goharian, E.; Baalousha, M. Identification and quantification of anthropogenic nanomaterials in urban rain and runoff using single particle-inductively coupled plasma-time of flight-mass spectrometry. Environmental Science: Nano **2022**, 9, 714–729.

(10) Dia, M.; Peyneau, P.-E.; Courtier-Murias, D.; Béchet, B. Detection and quantification of nanoparticles in runoff from a highly trafficked urban motorway. Environmental Science: Nano **2025**, 10.1039.D4EN00552J.

(11) Gondikas, A. P.; Kammer, F. v. d.; Reed, R. B.; Wagner, S.; Ranville, J. F.; Hofmann, T. Release of TiO2 Nanoparticles from Sunscreens into Surface Waters: A One-Year Survey at the Old Danube Recreational Lake. Environmental Science & Technology **2014**, 48, 5415–5422, Publisher: American Chemical Society.

(12) Phalyvong, K.; Sivry, Y.; Pauwels, H.; Gélabert, A.; Tharaud, M.; Wille, G.; Bourrat, X.; Ranville, J. F.; Benedetti, M. F. Assessing CeO2 and TiO2 Nanoparticle Concentrations in the Seine River and Its Tributaries Near Paris. Frontiers in Environmental Science **2021**, 8, 1–14, Publisher: Frontiers.

(13) Phalyvong, K.; Sivry, Y.; Pauwels, H.; Gélabert, A.; Tharaud, M.; Wille, G.; Bourrat, X.; Benedetti, M. F. Occurrence and Origins of Cerium Dioxide and Titanium Dioxide Nanoparticles in the Loire River (France) by Single Particle ICP-MS and FEG-SEM Imaging. Frontiers in Environmental Science **2020**, 8, 1–14, Publisher: Frontiers.

(14) Gallego-Urrea, J. A.; Hammes, J.; Cornelis, G.; Hassellöv, M. Coagulation and sedimentation of gold nanoparticles and illite in model natural waters: Influence of initial particle concentration. NanoImpact **2016**, 3-4, 67–74.

(15) Ribeiro, F.; Gallego-Urrea, J. A.; Jurkschat, K.; Crossley, A.; Hassellöv, M.; Taylor, C.; Soares, A. M.; Loureiro, S. Silver nanoparticles and silver nitrate induce high toxicity to Pseudokirchneriella subcapitata, Daphnia magna and Danio rerio. Science of The Total Environment **2014**, 466-467, 232–241.

(16) Arvidsson, R.; Molander, S.; Sandén, B. A.; Hassellöv, M. Challenges in Exposure Modeling of Nanoparticles in Aquatic Environments. Human and Ecological Risk Assessment: An International Journal **2011**, 17, 245–262.

(17) Lin, D.; Tian, X.; Wu, F.; Xing, B. Fate and Transport of Engineered Nanomaterials in the Environment. Journal of Environmental Quality **2010**, 39, 1896–1908.

(18) Baalousha, M. Aggregation and disaggregation of iron oxide nanoparticles: Influence of particle concentration, pH and natural organic matter. Science of The Total Environment **2009**, 407, 2093–2101.

(19) Barbero, F.; Mayall, C.; Drobne, D.; Saiz-Poseu, J.; Bastús, N. G.; Puntes, V. Formation and evolution of the nanoparticle environmental corona: The case of Au and humic acid. Science of The Total Environment **2021**, 768, 144792.

(20) Tipping, E.; Higgins, D. C. The effect of adsorbed humic substances on the colloid stability of haematite particles. Colloids and Surfaces **1982**, 5, 85–92.

(21) Zhang, Y.; Chen, Y.; Westerhoff, P.; Crittenden, J. Impact of natural organic matter and divalent cations on the stability of aqueous nanoparticles. Water Research **2009**, 43, 4249–4257.

(22) Dai, H.; Sun, T.; Han, T.; Li, X.; Guo, Z.; Wang, X.; Chen, Y. Interactions between cerium dioxide nanoparticles and humic acid: Influence of light intensities and molecular weight fractions. Environmental Research **2021**, 195, 110861.

(23) Hui, C.; Zhang, Y.; Ni, X.; Cheng, Q.; Zhao, Y.; Zhao, Y.; Du, L.; Jiang, H. Interactions of iron-based nanoparticles with soil dissolved organic matter: adsorption, aging, and effects on hexavalent chromium removal. Journal of Hazardous Materials **2021**, 406, 124650.

(24) Yi, Y.; Wu, J.; Tu, G.; Zhao, D.; Fang, Z.; Tsang, P. E. The humic acid influenced the behavior and reactivity of Ni/Fe nanoparticles in the removal of deca-brominated diphenyl ether from aqueous solution. Environmental Science and Pollution Research **2019**, 26, 10136–10147.

(25) Shi, J.; Ye, J.; Fang, H.; Zhang, S.; Xu, C. Effects of Copper Oxide Nanoparticles on Paddy Soil Properties and Components. Nanomaterials **2018**, 8, 839.

(26) Van Hoecke, K.; De Schamphelaere, K.; Van Der Meeren, P.; Smagghe, G.; Janssen, C. Aggregation and ecotoxicity of CeO2 nanoparticles in synthetic and natural waters with variable pH, organic matter concentration and ionic strength. Environmental Pollution **2011**, 159, 970–976.

(27) Masoom, H.; Courtier-Murias, D.; Farooq, H.; Soong, R.; Kelleher, B. P.; Zhang, C.; Maas, W. E.; Fey, M.; Kumar, R.; Monette, M.; Stronks, H. J.; Simpson, M. J.; Simpson, A. J. Soil Organic Matter in Its Native State: Unravelling the Most Complex Biomaterial on Earth. Environmental Science & Technology **2016**, 50, 1670–1680.

(28) Yu, S.; Liu, J.; Yin, Y.; Shen, M. Interactions between engineered nanoparticles and dissolved organic matter: A review on mechanisms and environmental effects. Journal of Environmental Sciences **2018**, 63, 198–217.

(29) Hyung, H.; Kim, J.-H. Natural Organic Matter (NOM) Adsorption to Multi-Walled Carbon Nanotubes: Effect of NOM Characteristics and Water Quality Parameters. Environmental Science & Technology **2008**, 42, 4416–4421.

(30) Sánchez-Cortés, S.; Francioso, O.; Ciavatta, C.; García-Ramos, J.; Gessa, C. pH-Dependent adsorption of fractionated peat humic substances on different silver colloids studied by surface-enhanced Raman spectroscopy. Journal of Colloid and Interface Science **1998**, 198, 308–318.

(31) Schubert, J.; Chanana, M. Coating Matters: Review on Colloidal Stability of Nanoparticles with Biocompatible Coatings in Biological Media, Living Cells and Organisms. Current Medicinal Chemistry **2018**, 25, 4553–4586.

(32) Grillo, R.; Rosa, A. H.; Fraceto, L. F. Engineered nanoparticles and organic matter: A review of the state-of-the-art. Chemosphere **2015**, 119, 608–619.

(33) Ju-Nam, Y.; Lead, J. R. Manufactured nanoparticles: An overview of their chemistry, interactions and potential environmental implications. Science of The Total Environment **2008**, 400, 396–414.

(34) Murugadoss, A.; Khan, A.; Chattopadhyay, A. Stabilizer specific interaction of gold nanoparticles with a thermosensitive polymer hydrogel. Journal of Nanoparticle Research **2010**, 12, 1331–1348.

(35) Shaterabadi, Z.; Nabiyouni, G.; Soleymani, M. High impact of *in situ* dextran coating on biocompatibility, stability and magnetic properties of iron oxide nanoparticles. Materials Science and Engineering: C **2017**, 75, 947–956.

(36) Aubrun Fulbert, C. et al. Nanoscintillator Coating: A Key Parameter That Strongly Impacts Internalization, Biocompatibility, and Therapeutic Efficacy in Pancreatic Cancer Models. Small Science **2024**, 4, 2400041, _eprint: https://onlinelibrary.wiley.com/doi/pdf/10.1002/smsc.202400041.

(37) Liu, L.; Bai, X.; Martikainen, M.-V.; Kårlund, A.; Roponen, M.; Xu, W.; Hu, G.; Tasciotti, E.; Lehto, V.-P. Cell membrane coating integrity affects the internalization mechanism of biomimetic nanoparticles. Nature Communications **2021**, 12, 5726.

(38) Pallem, V. L.; Stretz, H. A.; Wells, M. J. M. Evaluating Aggregation of Gold Nanoparticles and Humic Substances Using Fluorescence Spectroscopy. Environmental Science & Technology **2009**, 43, 7531–7535, Publisher: American Chemical Society.

(39) Lau, B. L. T.; Hockaday, W. C.; Ikuma, K.; Furman, O.; Decho, A. W. A preliminary assessment of the interactions between the capping agents of silver nanoparticles and environmental organics. Colloids and Surfaces A: Physicochemical and Engineering Aspects **2013**, 435, 22–27.

(40) Liu, J.; Legros, S.; von der Kammer, F.; Hofmann, T. Natural Organic Matter Concentration and Hydrochemistry Influence Aggregation Kinetics of Functionalized Engineered Nanoparticles. Environmental Science & Technology **2013**, 47, 4113–4120, Publisher: American Chemical Society.

(41) Diegoli, S.; Manciulea, A. L.; Begum, S.; Jones, I. P.; Lead, J. R.; Preece, J. A. Interaction between manufactured gold nanoparticles and naturally occurring organic macromolecules. Science of The Total Environment **2008**, 402, 51–61.

(42) Dong, H.; Lo, I. M. C. Influence of humic acid on the colloidal stability of surface-modified nano zero-valent iron. Water Research **2013**, 47, 419–427.

(43) Chekli, L.; Phuntsho, S.; Roy, M.; Shon, H. K. Characterisation of Fe-oxide nanoparticles coated with humic acid and Suwannee River natural organic matter. Science of The Total Environment **2013**, 461-462, 19–27.

(44) Hitchman, A.; Sambrook Smith, G. H.; Ju-Nam, Y.; Sterling, M.; Lead, J. R. The effect of environmentally relevant conditions on PVP stabilised gold nanoparticles. Chemosphere **2013**, 90, 410–416.

(45) Sun, X.-D.; Ma, J.-Y.; Feng, L.-J.; Duan, J.-L.; Xie, X.-M.; Zhang, X.-H.; Kong, X.; Ding, Z.; Yuan, X.-Z. Magnetite nanoparticle coating chemistry regulates root uptake

pathways and iron chlorosis in plants. Proceedings of the National Academy of Sciences **2023**, 120, e2304306120.

(46) Stankus, D. P.; Lohse, S. E.; Hutchison, J. E.; Nason, J. A. Interactions between Natural Organic Matter and Gold Nanoparticles Stabilized with Different Organic Capping Agents. Environmental Science & Technology **2011**, 45, 3238–3244.

(47) Tanaka, T. Functional groups and reactivity of size-fractionated Aldrich humic acid. Thermochimica Acta **2012**, 532, 60–64.

(48) Boguta, P.; D'Orazio, V.; Senesi, N.; Sokołowska, Z.; Szewczuk-Karpisz, K. Insight into the interaction mechanism of iron ions with soil humic acids. The effect of the pH and chemical properties of humic acids. Journal of Environmental Management **2019**, 245, 367–374.

(49) Saalidong, B. M.; Aram, S. A.; Otu, S.; Lartey, P. O. Examining the dynamics of the relationship between water pH and other water quality parameters in ground and surface water systems. PloS One **2022**, 17, e0262117.

(50) City of London Sifton Bog Environmentally Significant Area Conservation Master Plan 2009–2019; 2009; Chapter 4.

(51) Wu, F. C.; Evans, R. D.; Dillon, P. J. Separation and Characterization of NOM by High-Performance Liquid Chromatography and On-Line Three-Dimensional Excitation Emission Matrix Fluorescence Detection. Environmental Science & Technology **2003**, 37, 3687–3693, Publisher: American Chemical Society.

(52) Sierra, M.; Giovanela, M.; Parlanti, E.; Soriano-Sierra, E. Fluorescence fingerprint of fulvic and humic acids from varied origins as viewed by single-scan and excitation/emission matrix techniques. Chemosphere **2005**, 58, 715–733.

(53) Hudson, N.; Baker, A.; Reynolds, D. Fluorescence analysis of dissolved organic matter in natural, waste and polluted waters—a review. River Research and Applications **2007**, 23, 631–649.

(54) Woods, G. C.; Simpson, M. J.; Koerner, P. J.; Napoli, A.; Simpson, A. J. HILIC-NMR: Toward the Identification of Individual Molecular Components in Dissolved Organic Matter. Environmental Science & Technology **2011**, 45, 3880–3886, Publisher: American Chemical Society.

(55) Lakowicz, J. R. Principles of fluorescence spectroscopy, third edition, corrected at 4. printing ed.; Springer: New York, NY, 2010.

(56) Tanwar, A. S.; Parui, R.; Garai, R.; Chanu, M. A.; Iyer, P. K. Dual "Static and Dynamic" Fluorescence Quenching Mechanisms Based Detection of TNT via a Cationic Conjugated Polymer. ACS Measurement Science Au **2022**, 2, 23–30.

(57) Gehlen, M. H. The centenary of the Stern-Volmer equation of fluorescence quenching: From the single line plot to the SV quenching map. Journal of Photochemistry and Photobiology C: Photochemistry Reviews **2020**, 42, 100338.

(58) Mátyus, L.; Szöllősi, J.; Jenei, A. Steady-state fluorescence quenching applications for studying protein structure and dynamics. Journal of Photochemistry and Photobiology B: Biology **2006**, 83, 223–236.

(59) Tonet, M. Fluorescence Quenching & the Stern-Volmer Plot.

(60) Naik, A.; Naik, L.; Kadadevarmath, J.; Pal, H.; Rao, V. Fluorescence quenching of anthrylvinyl acetate by carbon tetrachloride. Journal of Photochemistry and Photobiology A: Chemistry **2010**, 214, 145–151.

(61) Veeralakshmi, S.; Sabapathi, G.; Nehru, S.; Venuvanalingam, P.; Arunachalam, S. Surfactant–cobalt(III) complexes: The impact of hydrophobicity on interaction with HSA

and DNA – insights from experimental and theoretical approach. Colloids and Surfaces B: Biointerfaces **2017**, 153, 85–94.

(62) Gan, L.-h.; Yan, Z.-r.; Ma, Y.-f.; Zhu, Y.-y.; Li, X.-y.; Xu, J.; Zhang, W. pH dependence of the binding interactions between humic acids and bisphenol A - A thermodynamic perspective. Environmental Pollution **2019**, 255, 113292.

(63) Zhang, Y.-Z.; Zhou, B.; Liu, Y.-X.; Zhou, C.-X.; Ding, X.-L.; Liu, Y. Fluorescence Study on the Interaction of Bovine Serum Albumin with P-Aminoazobenzene. Journal of Fluorescence **2008**, 18, 109–118.

(64) Lissi, E.; Calderón, C.; Campos, A. Evaluation of the Number of Binding Sites in Proteins from their Intrinsic Fluorescence: Limitations and Pitfalls. Photochemistry and Photobiology **2013**, 89, 1413–1416.

(65) Yan, Z.-r.; Meng, H.-s.; Yang, X.-y.; Zhu, Y.-y.; Li, X.-y.; Xu, J.; Sheng, G.-p. Insights into the interactions between triclosan (TCS) and extracellular polymeric substance (EPS) of activated sludge. Journal of Environmental Management **2019**, 232, 219–225.

(66) Hu, Y.-J.; Liu, Y.; Wang, J.-B.; Xiao, X.-H.; Qu, S.-S. Study of the interaction between monoammonium glycyrrhizinate and bovine serum albumin. Journal of Pharmaceutical and Biomedical Analysis **2004**, 36, 915–919.

(67) Ross, P. D.; Subramanian, S. Thermodynamics of protein association reactions: forces contributing to stability. Biochemistry **1981**, 20, 3096–3102, Publisher: American Chemical Society.

(68) Nakashima, K.; Xing, S.; Gong, Y.; Miyajima, T. Characterization of humic acids by two-dimensional correlation fluorescence spectroscopy. Journal of Molecular Structure **2008**, 883-884, 155–159.

(69) Zhu, G.; Yin, J. Fluorescence Quenching of Humic Acid by Coated Metallic Silver Particles. Journal of Fluorescence **2017**, 27, 1233–1243.

(70) Wang, L.; Li, H.; Yang, Y.; Zhang, D.; Wu, M.; Pan, B.; Xing, B. Identifying structural characteristics of humic acid to static and dynamic fluorescence quenching of phenanthrene, 9-phenanthrol, and naphthalene. Water Research **2017**, 122, 337–344.

(71) Li, H.; McKay, G. Fluorescence Quenching of Humic Substances and Natural Organic Matter by Nitroxide Free Radicals. Environmental Science & Technology **2023**, 57, 719–729.

(72) Dragan, A. I.; Read, C. M.; Crane-Robinson, C. Enthalpy–entropy compensation: the role of solvation. European Biophysics Journal **2017**, 46, 301–308.

(73) Loosli, F.; Vitorazi, L.; Berret, J.-F.; Stoll, S. Isothermal titration calorimetry as a powerful tool to quantify and better understand agglomeration mechanisms during interaction processes between TiO_2 nanoparticles and humic acids. Environmental Science: Nano **2015**, 2, 541–550.

(74) de Melo, B. A. G.; Motta, F. L.; Santana, M. H. A. Humic acids: Structural properties and multiple functionalities for novel technological developments. Materials Science and Engineering: C **2016**, 62, 967–974.

(75) Tan, K. H. Humic Matter in Soil and the Environment: Principles and Controversies, Second Edition, 2nd ed.; CRC Press: Boca Raton, 2014.

(76) Ritchie, J. D.; Perdue, E. M. Proton-binding study of standard and reference fulvic acids, humic acids, and natural organic matter. Geochimica et Cosmochimica Acta **2003**, 67, 85–96.

(77) Dia, M.; Farjon, J.; Raveleau, C.; Simpson, A.; Peyneau, P.-E.; Bechet, B.; Courtier-Murias, D. Understanding the Interactions of Nanoparticles and Dissolved Organic

Matter at the Molecular Level by 1H 2D Multi-Exponential Transverse Relaxation NMR Spectroscopy. Magnetic Resonance in Chemistry **2025**, 63, 63–48.

(78) Lan, T.; Wu, P.; Liu, Z.; Stroet, M.; Liao, J.; Chai, Z.; Mark, A. E.; Liu, N.; Wang, D. Understanding the Effect of pH on the Solubility and Aggregation Extent of Humic Acid in Solution by Combining Simulation and the Experiment. Environmental Science & Technology **2022**, 56, 917–927, Publisher: American Chemical Society.

(79) Terashima, M.; Fukushima, M.; Tanaka, S. Influence of pH on the surface activity of humic acid: micelle-like aggregate formation and interfacial adsorption. Colloids and Surfaces A: Physicochemical and Engineering Aspects **2004**, 247, 77–83.

(80) Xie, L.; Lu, Q.; Mao, X.; Wang, J.; Han, L.; Hu, J.; Lu, Q.; Wang, Y.; Zeng, H. Probing the intermolecular interaction mechanisms between humic acid and different substrates with implications for its adsorption and removal in water treatment. Water Research **2020**, 176, 115766.

(81) Longstaffe, J. G.; Courtier-Murias, D.; Simpson, A. J. The pH-dependence of organofluorine binding domain preference in dissolved humic acid. Chemosphere **2013**, 90, 270–275.

(82) Esfahani, M. R.; Pallem, V. L.; Stretz, H. A.; Wells, M. J. M. Humic acid disaggregation with/of gold nanoparticles: Effects of nanoparticle size and pH. Environmental Nanotechnology, Monitoring & Management **2016**, 6, 54–63.

(83) Brigante, M.; Zanini, G.; Avena, M. On the dissolution kinetics of humic acid particles. Effect of monocarboxylic acids. Chemosphere **2008**, 71, 2076–2081.

(84) Piccolo, A.; Conte, P.; Cozzolino, A. Effects of mineral and monocarboxylic acids on the molecular association of dissolved humic substances. European Journal of Soil Science **1999**, 50, 687–694.